W-band photonic-wireless link with a Schottky diode envelope detector and bend insensitive fiber

Rommel, Simon; Cavalcante, Lucas Costa Pereira; Quintero, Alexander Galvis; Mishra, Arvind K.; Vegas Olmos, Juan José; Tafur Monroy, Idelfonso

Published in:
Optics Express

Link to article, DOI:
10.1364/OE.24.011312

Publication date:
2016

Document Version
Peer reviewed version

W-band photonic-wireless link with a Schottky diode envelope detector and bend insensitive fiber

Simon Rommel,[1,*] **Lucas C. P. Cavalcante,**[1] **Alexander G. Quintero,**[2] **Arvind K. Mishra,**[3] **J. J. Vegas Olmos**[1] **and Idelfonso Tafur Monroy**[1]

[1]*Department of Photonics Engineering, Technical University of Denmark, Ørsteds Plads, 2800 Kgs. Lyngby, Denmark*
[2]*GIDATI, Telecommunications Engineering Faculty, Universidad Pontificia Bolivariana, Campus de Laureles, Medellín, Colombia*
[3]*Centre of Excellence, Sterlite Technologies Limited, E1-E3, MIDC Waluj, Aurangabad 431 136, Maharashtra, India*
[*]*sirem@fotonik.dtu.dk*

Abstract: The performance and potential of a W-band radio-over-fiber link is analyzed, including a characterization of the wireless channel. The presented setup focuses on minimizing complexity in the radio frequency domain, using a passive radio frequency transmitter and a Schottky diode based envelope detector. Performance is experimentally validated with carriers at 75–87GHz over wireless distances of 30–70m. Finally the necessity for and impact of bend insensitive fiber for on-site installation are discussed and experimentally investigated.

OCIS codes: (060.5625) Radio frequency photonics; (060.4510) Optical communications.

References and links

1. X. Pang, A. Lebedev, J. J. Vegas Olmos, and I. Tafur Monroy, "Multigigabit W-band (75-110 GHz) bidirectional hybrid fiber-wireless systems in access networks," J. Lightwave Technol. **32**, 3983–3990 (2014).
2. T. Pfeiffer, "Next generation mobile fronthaul architectures," in *Proc. OFC 2015* (OSA, 2015), pp. 1–3.
3. H. Yang, A. Ng'oma, B. Shih, A. Gowda, and L. Kazovsky, "Fiber-based solutions for in-door multi-Gbit/s wireless access," in *Proc. OFC 2015* (OSA, Los Angeles, 2015), paper W3F.1.
4. J. J. Vegas Olmos, T. Kuri, T. Sono, K. Tamura, H. Toda, and K.-i. Kitayama, "Wireless and optical-integrated access network with peer-to-peer connection capability," IEEE Photonics Technol. Lett. **20**, 1127–1129 (2008).
5. K.-i. Kitayama, T. Kuri, J. J. Vegas Olmos, and H. Toda, "Fiber-wireless networks and radio-over-fibre technique," in *Proc. CLEO/QELS 2008* (OSA, 2008), pp 1–2..
6. J. Wells, "Faster than fiber: The future of multi-G/s wireless," IEEE Microw. Mag. **10**, 104–112 (2009).
7. J. J. Vegas Olmos, T. Kuri, and K.-i. Kitayama, "Reconfigurable radio-over-fiber networks: Multiple-access functionality directly over the optical layer," IEEE Trans. Microw. Theory Tech. **58**, 3001–3010 (2010).
8. W.-J. Jiang, H. Yang, Y.-M. Yang, C.-T. Lin, and A. Ng'oma, "40 Gb/s RoF signal transmission with 10 m wireless distance at 60 GHz," in *OFC/NFOEC 2012* (OSA, 2012), pp. 1–3.
9. A. Lebedev, X. Pang, J. J. Vegas Olmos, S. Forchhammer, and I. Tafur Monroy, "Simultaneous 60-GHz RoF transmission of lightwaves emitted by ECL, DFB, and VCSEL," IEEE Photonics Technol. Lett. **26**, 733–736 (2014).
10. C.-H. Li, M.-F. Wu, C.-H. Lin, and C.-T. Lin, "W-band OFDM RoF system with simple envelope detector down-conversion," in *Proc. OFC 2015* (OSA, 2015), pp. 1–3.
11. S. Rommel, L. C. P. Cavalcante, J. J. Vegas Olmos, and I. Tafur Monroy, "Low RF complexity photonically enabled indoor and building-to-building w-band wireless link," in *Proc. ACP 2015* (OSA, 2015), paper AM1B.7.
12. S. Koenig, F. Boes, D. Lopez-Diaz, J. Antes, R. Henneberger, R. M. Schmogrow, D. Hillerkuss, R. Palmer, T. Zwick, C. Koos, W. Freude, O. Ambacher, I. Kallfass, and J. Leuthold, "100 Gbit/s wireless link with mm-wave photonics," in *Proc. OFC 2013* (OSA, 2013), pp 1–3.

13. H. Xu, V. Kukshya, and T. S. Rappaport, "Spatial and temporal characteristics of 60-GHz indoor channels," IEEE J. Sel. Areas Commun. **20**, 620–630 (2002).
14. A. P. Garcia, W. Kotterman, R. S. Thoma, U. Trautwein, D. Bruckner, W. Wirnitzer, and J. Kunisch, "60 GHz in-cabin real-time channel sounding," in *Proc. ChinaCOM 2009* (IEEE, 2009), pp 1–5.
15. S. Rommel, A. Galvis Quintero, L. C. P. Cavalcante, J. J. Vegas Olmos, and I. Tafur Monroy, "Channel characterization for high-speed W-band wireless communication links," in *Proc. OECC 2015* (IEEE, 2015), pp. 1–3.
16. A. Stöhr, O. Cojucari, F. van Dijk, G. Carpintero, T. Tekin, S. Formont, I. Flammia, V. Rymanov, B. Khani, and R. Chuenchom, "Robust 71-76 GHz radio-over-fiber wireless link with high-dynamic range photonic assisted transmitter and laser phase-noise insensitive SBD receiver," in *Proc. OFC 2014* (OSA, 2014), paper M2D.4.
17. R. Chuenchom, X. Zou, V. Rymanov, B. Khani, M. Steeg, S. Dülme, S. Babiel, A. Stöhr, J. Honecker, and A. G. Steffan, "Integrated 110 GHz coherent photonic mixer for CRoF mobile backhaul links," in *Proc. MWP 2015* (IEEE, 2015), paper 1–4.
18. S. Rommel, S. Rodriguez, L. Chorchos, E. P. Grakhova, A. K. Sultanov, J. P. Turkiewicz, J. J. Vegas Olmos, and I. Tafur Monroy, "225m outdoor W-band radio-over-fiber link using an optical SFP+ module," in *Proc. OFC 2016* (OSA, 2016), paper Th2A.16.
19. C. Lim, A. Nirmalathas, M. Bakaul, K.-L. Lee, D. Novak, and R. Waterhouse, "Mitigation strategy for transmission impairments in millimeter-wave radio-over-fiber networks," J. Opt. Netw. **8**, 201–214 (2009).
20. A. Lebedev, J. J. Vegas Olmos, X. Pang, S. Forchhammer, and I. Tafur Monroy, "Demonstration and comparison study for V- and W-band real-time high-definition video delivery in diverse fiber-wireless infrastructure," Fiber Integrated Opt. **32**, 93–104 (2013).
21. M. Morant, A. Macho, and R. Llorente, "Optical fronthaul of LTE-advanced MIMO by spatial multiplexing in multicore fiber," in *Proc. OFC 2015* (OSA, 2015), paper W1F.6.
22. D. Z. Chen, W. R. Belben, J. B. Gallup, C. Mazzali, P. Dainese, and T. Rhyne, "Requirements for bend insensitive fibers for Verizon's FiOS and FTTH applications," in *Proc. OFC 2008* (IEEE, 2008), pp. 1–7.
23. S. Rommel, L. C. P. Cavalcante, J. J. Vegas Olmos, I. Tafur Monroy, and A. K. Mishra, "Requirements for bend insensitive fiber in millimeter-wave fronthaul systems," in *Proc. MWP 2015* (IEEE, 2015), pp. 1–4.
24. B. Sklar, "Rayleigh fading channels in mobile digital communication systems - Part I: characterization," IEEE Commun. Mag. **35**, 90–100 (1997).
25. T. S. Rappaport, *Wireless Communications: Principles and Practice*, 2nd ed. (Prentice Hall, 2002).
26. I. Oppermann, M. Hämäläinen, and J. Iinatti, eds., *UWB: Theory and Applications* (John Wiley and Sons, 2004).

1. Introduction

The immense growth in the usage of mobile and wireless data – driven by the use of bandwidth intensive applications on mobile consumer devices – has lead to an increasing demand for high-speed multi-gigabit wireless connections. In order to accommodate this need, new strategies must be employed both in direct wireless access and in wireless point-to-point links leading up to the access point, such as in mobile front- and backhaul, wireless building-to-building links or wireless bridges over obstacles [1–4]. A migration away from the already congested conventional wireless bands and towards higher frequency bands – such as the millimeter-wave (mmW) region – is generally considered a necessity to support the required bandwidths and mmW radio-over-fiber (RoF) links have been identified as a key candidate, combining the advantages of optical and wireless communications [4–7].

Hybrid photonic-wireless links in the IEEE V- (50–75 GHz) [3, 8, 9] and W-bands (75–110 GHz) [1,10,11] and beyond [12] have been demonstrated with a variety of setups, achieving transmission distances ranging from a few to multiple hundred meters. While carriers at 60 GHz have been in focus for Gbit/s indoor wireless [3, 9] this region is affected by a large peak in atmospheric absorption [6], severely limiting it to short-range transmissions. The W-band however does not share this limitation and may thus be a candidate for indoor and building-to-building transmission scenarios as well as mobile front- and backhaul [1–3] as shown in Fig. 1.

To ensure the feasibility of mmW wireless links in all the aforementioned scenarios however, three issues require additional attention and are addressed in this article:

- *characterization of the wireless channel*: most efforts for channel characterization and modelling have regarded frequencies in and below V-band or only estimated path loss

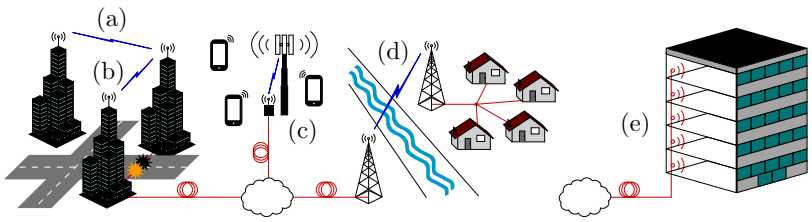

Fig. 1. Network scenarios for the hybrid fiber-wireless link. (a)–(d) outdoor medium distance links: (a) building-to-building communication, (b) recovery and protection of fiber links, (c) mobile front-/backhaul, (d) spanning obstacles and providing broadband access to rural ares; (e) short-range indoor wireless distribution

[13, 14]. A characterization of the W-band wireless channel has been performed [15] and is presented in section 2.

- *complexity of the setup*: Gbit/s class W-band wireless transmissions reaching long distances have been performed with high complexity in both the optical and radio frequency (RF) domains; setups with reduced complexity employing envelope detection for (RF) downconversion were suggested [10, 16], but only recently [11, 17, 18] reached distances beyond 10 m wireless transmission. A setup with a passive RF transmitter and a Schottky diode based envelope detector to minimize complexity in the RF domain has been developed [11] and is presented in section 3. Section 4 presents experimental results, successfully transmitting 2.5 Gbit/s of data over wireless distances of 30 to 70 m with carriers at 75 to 87 GHz as shown in section 4.1.
- *fiber installation*: the requirements for fiber to be installed directly to the transmitting antenna have not been regarded; previous investigations have focussed on the transmission fiber and associated impairments [19, 20] or on capacity enhancements through fiber spatial multiplexing and multiple-input multiple-output (MIMO) RF transmission [21]. The necessity for bend insensitive fiber (BIF) for on-site installation is obvious and similar to the case of fiber-to-the-x [22, 23] and the impact of including it in the transmission line is analyzed and discussed in section 4.2.

Finally section 5 summarizes and concludes the article.

2. W-Band Wireless Channel Characterization

2.1. Wireless Channel Modelling

The characterization of the phenomena affecting communication signals during propagation in wireless systems is fundamental to the definition and development of the digital signal processing required for their compensation or mitigation. The manifestations of fading channels are commonly classified in two groups: large-scale and small-scale fading [24], with the former mainly due to the distance between the transmitting and receiving antennas, the given environment and the resulting attenuation, while the latter is described by a number of characteristics including the time and frequency responses of the channel.

Large-scale fading is characterized statistically by calculating the mean of the observed attenuation in dependence on transmission distance – path loss – and its variations around this mean – shadowing. While a variety of models for path loss estimation is found in the literature [25], two of the most commonly employed have been selected for comparison. The free-space loss model (FSL, referred to as Friis model) defines path loss as in (1), where d is the distance between transmitting and receiving antenna, f the carrier frequency and c the speed of light in

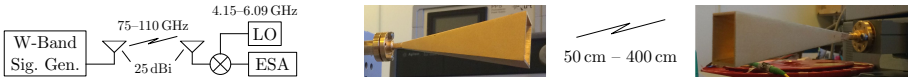

Fig. 2. Schematic of the experimental setup for W-band channel characterization and photograph of the pair of pyramidal waveguide horns. LO: local oscillator, ESA: electrical spectrum analyzer

vacuum.

$$FSL_{[dB]} = 10\log\left((4\pi df/c)^2\right) = 20\log(4\pi df/c) \tag{1}$$

The generic empirical path loss model (GEPL) in (2) expresses total path loss as the observed loss L_0 at a reference distance d_0 and a term dependent on both distance d and the path loss exponent n, with the latter adapting the model to the studied environment.

$$GEPL_{[dB]} = 10n\log(d/d_0) + L_0 \tag{2}$$

Shadowing is easily calculated from experimental path loss data as a random variable – the shadowing parameter (σ_S) – with log-normal distribution additive to path loss [25].

The small-scale fading behavior of a channel includes its frequency selectivity as well as possible multipath phenomena and is characterized by the respective associated parameters, including coherence bandwidth (B_c), root mean squared delay (τ_{rms}), Doppler shift (f_d) and coherence period (T_c) [24–26].

2.2. *Channel Measurement Setup and Raw Results*

For the characterization of a short distance indoor W-band wireless link a setup as depicted in Fig. 2 is used, in which a vector signal generator (VSG) in combination with a frequency sextupler generates the signal to be transmitted, while at the receiver the signal is down-converted to intermediate frequency (IF) using a harmonic mixer driven by a 4–6 GHz local oscillator (LO). The resulting received spectra and power levels are recorded on an electrical spectrum analyzer (ESA). Wireless transmission is based on a pair of pyramidal waveguide horn antennas with a mid-band gain of 25 dBi each.

In order to ensure reliability and comparability of the measurement results, the involved VSG and ESA were adjusted to give agreeing and consistent power readings and the frequency response of the mixer was accounted for according to manufacturer measurements; it should be noted however that not all uncertainty may be calibrated out of the setup and a certain effect of the equipments' response over frequency may affect the measurement results. For the antennas a flat frequency response is assumed across the entire sounded band.

A single-tone method as described in [26] is used to sweep the complete W-band spectrum with a 1 MHz resolution, recording received power levels at distances between 0.5 m and 4 m. The recorded data allows for both large and small scale analysis, but already in their raw form as shown in Fig. 3 gives a clear indication of the distance dependency of path loss; the reduced performance at the upper frequency edge of the analyzed band is caused by frequency limitations of the employed equipment.

2.3. *Large-Scale Fading Analysis*

The experimentally obtained W-band path loss values are compared to the predictions of the Friis model in Figs. 4(a) and 4(b) for distance and frequency dependency respectively. In both cases good agreement between prediction and experimental data is found although a loss over distance slightly higher than predicted by the Friis model is observed in Fig. 4(a), while in Fig. 4(b) the observed loss is marginally below the prediction of the Friis model especially for

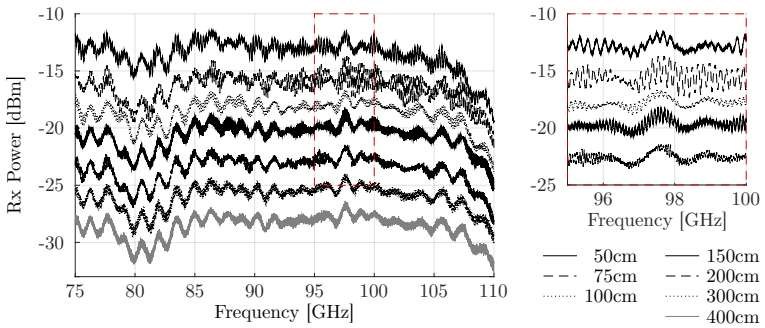

Fig. 3. Received power over frequency at distances of 0.5–4 m; close up: showing the aggregated effects of path loss, shadowing and small-scale fading

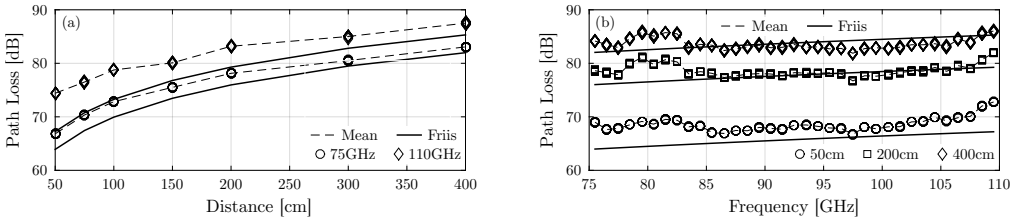

Fig. 4. Path loss over (a) distance and (b) frequency compared to predictions based on the Friis transmission equation (1)

the larger distances. With a mean error of 2.1 dB at 75 GHz and 4.3 dB at 110 GHz this confirms the Friis model to be a good model for the measured point-to-point link.

The path loss exponent (n) and shadowing parameter (σ_S) were calculated from the experimental data as discussed in [25], finding the GEPL to approximate the experimental data well for path loss exponents of $n \approx 2.2$ and $n \approx 2.5$ at 75 GHz and 110 GHz respectively, confirming the expectations for a short directive link in an indoor environment [25]. Due to the short distances and moderate directivity of the link, the observed shadowing is very small at 0.05 dB and 0.12 dB for 75 GHz and 110 GHz respectively.

Overall it is clear that for short distance links under the present conditions the dependency of path loss on distance is by far the dominant effect, with an increase in distance from 0.5 m to 4 m resulting in an additional 13.1 dB to 16.2 dB of path loss depending on frequency. This frequency dependency of path loss seen in Fig. 4(b) implies an increase in path loss of 3.8 dB at 0.5 m, 3.3 dB at 2 m and 1.9 dB at 4 m for an increase of frequency from 75 GHz to 110 GHz. While small in comparison to the impact of varying distance and easily compensated in narrow band systems, such frequency dependent variations in path loss may be detrimental to signal integrity for systems with bandwidths as large as expected for future communication systems in W-band. Large-scale fading analysis of the channel is thus insufficient to describe the encountered channel effects in the required detail and small-scale fading analysis becomes a necessity.

2.4. Small-Scale Fading Analysis

For signals with bandwidths of multiple GHz – as expected in future systems and when using photonic upconversion – the relevant channels are likely to be characterized by a multipath rich profile, resulting in significantly lower power levels for each multipath component. Analysis of the experimentally obtained S_{21} parameters using the inverse fast Fourier transformation (IFFT) and the Hermitian method [26] allows calculation of the frequency response of the channel,

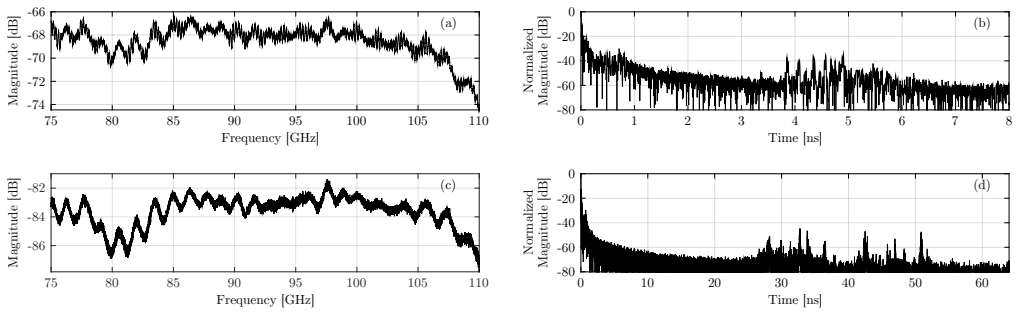

Fig. 5. Wireless channel frequency ((a), (c)) and time ((b), (d)) response at 50 cm ((a), (b)) and 400 cm ((c), (d)) transmission distance

shown in Figs. 5(a) and 5(c) for distances of 0.5 m and 4 m respectively. Except for a dip around 80 GHz – likely due to a dip in efficiency of the frequency generation setup – and a drop near the upper end of the band caused by the operational limits of the involved devices, the channel frequency response is very uniform across the whole band, with its magnitude strongly determined by path loss due to the directivity of the link.

The normalized time response of the channel – shown in Figs. 5(b) and 5(d) for distances of 0.5 m and 4 m respectively – represents good approximation of the power delay profile (PDP) of the channel [26], allowing the calculation of the corresponding root mean square delay τ_{rms} and coherence bandwidth B_c. Assuming a threshold of −60 dBm for the selection of significant multipath components, values of $\tau_{rms} = 0.16\,\text{ns}$ and $B_c = 6.3\,\text{GHz}$ are obtained for $d = 0.5\,\text{m}$ while at $d = 4\,\text{m}$ values of $\tau_{rms} = 0.40\,\text{ns}$ and $B_c = 2.5\,\text{GHz}$ are found. It is clear that with increasing transmission distance the delays grow – as the difference in distance traveled by the multipath components increases – and hence coherence bandwidth reduces. For a modulated signal of 6 GHz bandwidth this would indicate that while at 0.5 m the encountered channel may be quasi flat, at 4 m severe frequency fading will cause a significant degradation of signal quality. The assumed threshold of −60 dBm may appear low when considering observed path loss and typical receiver sensitivities and with a higher threshold all significant components might belong to the first tap of the PDP; when considering links with lower directivity or the introduction of point-to-multipoint transmission however, the limitations posed by multipath propagation will be significant and may result in coherence bandwidths considerably smaller than those found.

2.5. Discussion

The results obtained from the channel characterization suggest that the well known models for path loss estimation – i.e. Friis and the GEPL models – retain their validity in predicting large-scale phenomena and received power levels. Multipath propagation effects have been observed to potentially pose limits on the usable signal bandwidths, depending on link directivity, the considered threshold level for the significance of multipath contributions and on whether transmission takes place in a point-to-point or point-to-multipoint scenario. The specific channel analyzed may be considered line-of-sight and – even though only covering short distances – the channel characteristics found may give an indication towards conditions for longer distance transmissions. This is especially the case if an increase in transmission distance is accompanied by an increase in antenna directivity, such as in the following sections where wireless distances of 30–70 m are covered by employing a pair of highly directive parabolic antennas.

While on one hand for short distance transmissions or systems with highly directive antennas the channel may be considered as line-of-sight only, for systems with low directivity on the

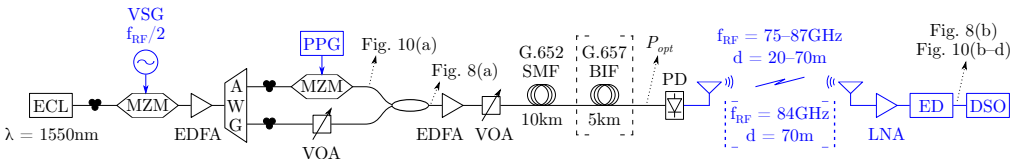

Fig. 6. Experimental setup for radio-over-fiber transmission and bend insensitive fiber analysis. ECL: external cavity laser, VSG: vector signal generator, MZM: Mach-Zehnder modulator, EDFA: erbium doped fiber amplifier, AWG: arrayed waveguide grating, PPG: pulse pattern generator, VOA: variable optical attenuator, SMF: standard single-mode fiber, BIF: bend insensitive fiber, PD: photodiode, LNA: low noise amplifier, ED: envelope detector, DSO: digital storage oscilloscope

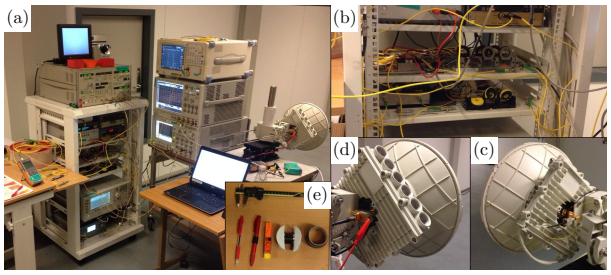

Fig. 7. (a) Portable laboratory setup with photonic upconversion, (b) rack-mounted optical setup, (c) transmit antenna with PD, (d) receive antenna with LNA and ED, (e) mandrels of different radii for bending analysis

other hand it may be necessary to compensate for the signal degradation resulting from path loss and shadowing – potentially through employing a degree of diversity, gaining additional uncorrelated estimates of the signal – and to mitigate the observed frequency selectivity, either through pre-processing or by applying equalization.

3. Low RF Complexity Fiber-Wireless Transmission System Setup

The radio-over-fiber (RoF) transmission system employed for the analysis of transmission performance and the study of mitigating fiber bending impacts through the use of bend insensitive fiber (BIF) is shown in Figs. 6 and 7. The setup consists of three distinct parts which in a deployment case would be geographically separate: (I) optical signal generation and modulation linked by optical fiber transmission to (II) optical to radio-frequency (RF) conversion linked by W-band RF transmission to (III) the receiver.

Signal generation – i.e. the left hand side of Fig. 6 – consists of an external cavity laser (ECL) at $\lambda = 1550\,\text{nm}$, followed by a Mach-Zehnder modulator (MZM) biased at its minimum transmission point and driven with a sinusoidal at $f_{RF}/2$ to generate two spectral lines spaced at f_{RF}. In order to allow performance analysis at different RF carrier frequencies the frequency of the driving signal is varied, generating line spacings of 75–87 GHz. The signal is amplified by 22 dB using an erbium doped fiber amplifier (EDFA) with a noise figure (NF) 5.8 dB and an arrayed waveguide grating (AWG) separates the two spectral lines, allowing to modulate one with data. A $2^{15} - 1$ bit long pseudo-random bit sequence (PRBS15) non-return-to-zero (NRZ) signal at speeds between 1 Gbit/s and 2.5 Gbit/s – generated with a pulse pattern generator (PPG) – directly drives the second MZM, biased in the linear part of its transmission curve for optimum extinction ratio. Two variable optical attenuators (VOAs) ensure equal power of the two arms and allow control over the output optical power. The experimental setup for signal

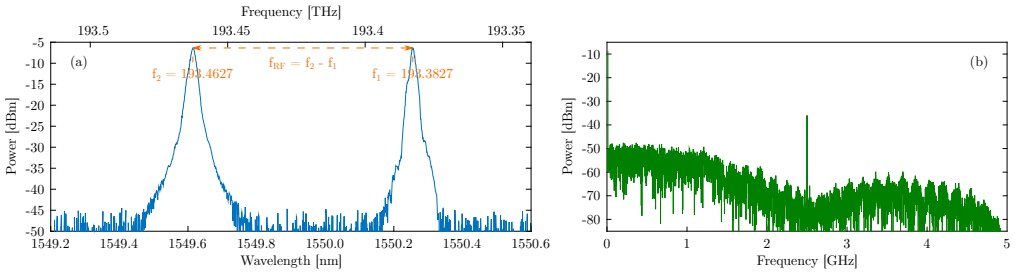

Fig. 8. Signal spectra: (a) Optical signal at the output of the 3 dB coupler before fiber transmission and photonic upconversion, for the generation of a signal with an 80 GHz carrier; (b) Received electrical spectrum after envelope detection of the 2.5 Gbit/s NRZ signal on an 84 GHz carrier and 70 m wireless transmission with $P_{opt} = 5$ dBm

generation is depicted in Fig. 7(b), while Fig. 8(a) shows the spectrum of the generated signal at the output of the coupler.

A second EDFA with a 4.3 dB NF amplifies the signal by 20 dB before it is transmitted through 10 km of ITU-T G.652 standard single-mode fiber (SMF) with one of three spool samples of 5 km Sterlite BIF added to the transmission line for the investigation of performance when subjected to macrobending. After fiber transmission the optical signal is converted to an RF signal by beating the two spectral lines on a photodiode (PD) with a nominal 3 dB bandwidth of 100 GHz and a responsivity of 0.5 A/W. The generated RF signal is transmitted without further amplification through a pair of parabolic antennas – shown in Figs. 7(c) and 7(d) – with a gain of 48 dBi each.

At the receiver site the signal is amplified by a low noise amplifier (LNA) providing 40 dB gain before down-conversion takes place in a Schottky diode based envelope detector (ED) with a 3 dB bandwidth of 3 GHz, yielding a baseband signal as shown in Fig. 8(b) for an exemplary case. Employing envelope detection rather than down-conversion with an electrical mixer alleviates the need for a local oscillator at the receiver and thus – together with the a passive wireless transmitter and only a single LNA at the receiver – minimizes complexity of the RF chain at both ends. Finally the received baseband signal is recorded using a digital storage oscilloscope (DSO) and bit-error rate (BER) values are determined through offline processing, consisting of simple thresholding and error counting over four recorded sequences with a length $>$2.5 Mbit each.

For the analysis of transmission performance the power incident on the PD is varied between 0–8 dBm through the use of the second VOA while wireless distance and carrier frequency are varied between 30–70 m and 75–87 GHz respectively. During the analysis of the effects of fiber bending and their mitigation through the use of BIF, carrier frequency and wireless distance are fixed to 84 GHz and 70 m respectively. Macrobending is induced by winding the different fiber samples for 1–10 turns around mandrels with radii between 5–15 mm – shown in Fig. 7(e) – and performance is analyzed by monitoring the resulting incident power on the PD with a 1 % tap and by recording BER values.

4. Experimental Results

4.1. W-Band Transmission Performance Analysis

The performance of the reduced RF complexity W-band photonic-wireless link is analyzed for wireless links of 30–70 m and utilizing carrier frequencies between 75–87 GHz, while the optical transmission link consists of 10 km SMF in all cases. Figure 9 shows BER as a function

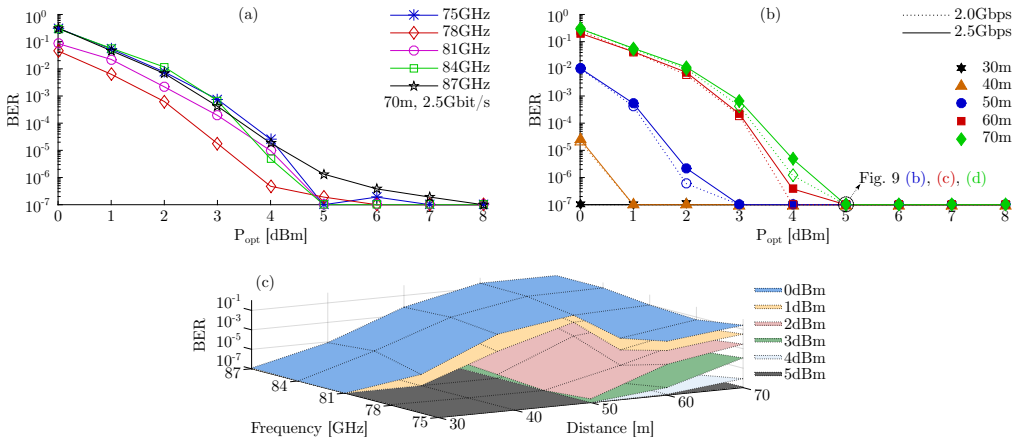

Fig. 9. Evolution of BER: (a) vs P_{opt} for different RF carrier frequencies at 2.5 Gbit/s and after 70 m wireless transmission, (b) vs P_{opt} for wireless transmission distances between 30 m and 70 m at data rates of 2 Gbit/s and 2.5 Gbit/s and with an RF carrier frequency of 84 GHz, (c) vs distance and carrier frequency for 0 dBm $\leq P_{opt} \leq$ 5 dBm

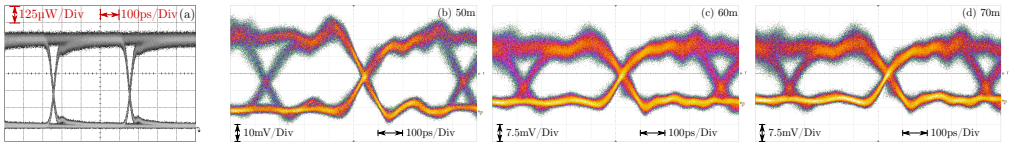

Fig. 10. Eye diagrams: (a) transmitted 2.5 Gbit/s NRZ signal, (b–d) received signal after envelope detection of the 2.5 Gbit/s NRZ signal on an 84 GHz carrier and 50–70 m wireless transmission with $P_{opt} = 5$ dBm

of power incident on the PD and compares performance dependency on wireless distance and carrier frequency. Figure 9(a) allows analysis of frequency dependency at a fixed distance and data rate, finding it to be low while following the trend predicted by the Friis model; with the additional free space loss amounting to only 1.3 dB when comparing RF carriers at 75 GHz and 87 GHz performance variations of the involved RF equipment clearly dominate when regarding frequency dependency.

Figure 9(b) details evolution of transmission performance over distance with a fixed carrier frequency of 84 GHz, while Fig. 10 shows corresponding transmitter and receiver eye diagrams for a fixed optical power of 5 dBm; Fig. 8(b) gives the received electrical spectrum after 70 m wireless transmission. It should be noted that in all of Fig. 9 a plotted BER of 10^{-7} indicates successful and error free transmission of four sequences with a length of >2.5 Mbit each. Assuming a BER of 10^{-6} as reference minimum, optical powers on the PD of 0.7 dBm and 4.4 dBm are found for distances of 40 m and 70 m respectively, translating into an increase in available RF power adequate to overcome the additional free space loss of 4.9 dB, while also allowing for a slightly less optimal alignment of the antennas at the larger distances.

Overall the system is found to be power limited, as is also seen in Fig. 9(c) with the surfaces – corresponding to optical powers on the PD – neatly nested and allowing different distance-frequency combinations depending on selected BER limit. With no error observed at 5 dBm and an additional 3 dB in optical power available it is expected that transmission distances beyond the mark of 100 m would be within reach of the system.

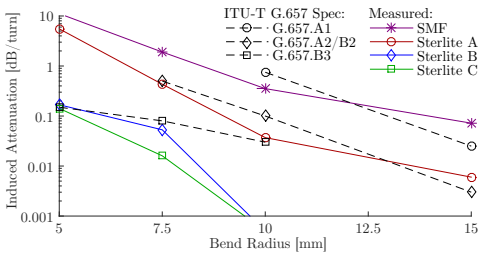

Fig. 11. Comparison of macrobending losses of Sterlite BIF fiber samples at 1550 nm with ITU-T G.657 A1, A/B2 and B3 specifications

4.2. Mitigation of Fiber Bending Impacts – Performance with Bend Insensitive Fiber

The first step in analyzing how BIF can help mitigate the impact of fiber bending is a comparison of macrobending loss of the different fibers under test with the specifications of ITU-T G.657 as shown in Fig. 11. As the number of turns in an installation may easily reach the equivalent of ten turns, the observed bending loss of SMF suggests minimum bending radii of 15 mm or above, depending on system power budget. With losses well below those required by ITU-T G.657.A1 and as much as an order of magnitude lower at radii of 10–15 mm than those of SMF, sample A allows significantly tighter radii. Samples B and C compare favorably to the requirements of G.657.A2/B2 and G.657.B3 respectively with sample C showing a five times lower loss at 7.5 mm radius, suggesting macrobending loss at this radius to be near negligible and radii down to 5 mm to be allowable while maintaining lower loss per turn values than SMF at 15 mm bending radius.

Further analysis of transmission performance is dependent on the system under test, but may give a good indication of the benefit obtained through the used of BIF. At a distance of 70 m and with a carrier of 84 GHz, setting $P_{opt} = 6$ dBm as reference power and assuming a required maximum BER of 10^{-6} suggests a margin for allowable loss through fiber bending of about 2 dB. Figures 12(a) and 12(c) show the dependency of system BER performance on the optical power P_{opt} incident on the PD at 1 Gbit/s and 2.5 Gbit/s respectively. Figures 12(b) and 12(d) visualize the corresponding numbers of turns at different radii that were found to be allowable with the different fiber samples while maintaining system performance with a BER $< 10^{-6}$, while setting a BER limit of 10^{-3} does not significantly alter the picture with only a single data point being changed for each of the data rates, as indicated by the $\triangledown$ and $\triangle$ in Figs. 12(b) and 12(d) respectively. Both clearly show the benefit with respect to bending tolerance that may be obtained with BIF and correspond well to the loss margin of 2 dB. It is clear that at radii of 10 mm G.657.A1 type fiber may sufficiently reduce the encountered macrobending losses, while for even smaller radii A2/B2 and B3 fibers may be required. While in the present case no difference was seen between samples B and C, an extrapolation of their encountered loss per turn values from Fig. 11 up to the loss margin suggests as many as 11 and 14 turns to be allowable at 5 mm, while at 7.5 mm up to 38 and 126 turns respectively are expected be possible without degrading system performance.

While the margin of 2 dB for allowable bending loss is specific to the assessed system and link, the indication of requiring BIF for radii of 10 mm and below is a general one as is the scale of the benefit to be obtained by the different fiber types. This serves to highlight the trade-off to be found between system parameters such as the available power budget and logistical challenges such as the required tolerance to bending and ease of installation on one side and economical considerations such as the additional cost of BIF on the other side.

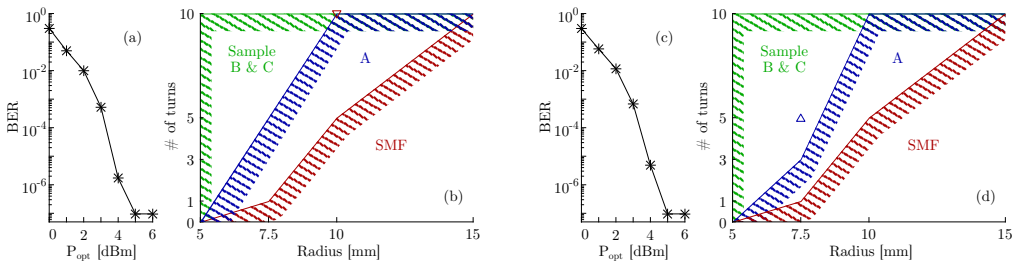

Fig. 12. BER vs P_{opt} without bending (a,b) and allowable numbers of turns at different radii (b,d) for a system performance with BER $< 10^{-6}$; wireless distance: 70 m, carrier frequency: 84 GHz. (a,b) at 1 Gbit/s ($\triangledown$: BER $= 2.0 \times 10^{-4}$ for 10 turns @ 10 mm with SMF fiber), (c,d) at 2.5 Gbit/s ($\triangle$: BER $= 2.5 \times 10^{-6}$ for 5 turns @ 7.5 mm with sample A)

5. Conclusions

The wireless channel in W-band was characterized and a radio-over-fiber transmission link with reduced complexity in the RF domain demonstrated, achieving successful transmission of a 2.5 Gbit/s signal. The wireless channel is found to be affected by multipath propagation and resulting impairments, however in the case of short distances or high link directivity it may be regarded as purely line-of-sight.

The complexity of the RoF link setup was reduced by employing a passive RF transmitter and a Schottky diode based envelope detector for signal downconversion, minimizing the number of required RF amplifiers and alleviating the need for RF mixers and a local oscillator at the receiver. Successful transmission is demonstrated for RF carriers at 75–87 GHz – i.e. the lower half of the W-band – and over wireless distances of 30–70 m, with distances of 100 m and beyond predicted to be achievable. The system is thus shown to be applicable in both indoor and outdoor scenarios, including building-to-building connections and mobile front- and backhaul.

Furthermore the performance impact of including bend insensitive fiber for on-site installation was experimentally analyzed, employing three samples of Sterlite bend insensitive fiber. A clear benefit in terms of tolerance to macrobending is found, with bend radii as small as 5 mm and more than ten turns allowable without significant degradation of system BER performance.

Through the reduction in complexity and the inclusion of bend insensitive fiber, the applicability of W-band hybrid photonic-wireless links as a key enabler for future wireless and mobile networks is highlighted and with the obtained transmission results their performance is experimentally confirmed.

Acknowledgments

This work was partly funded by the DFF FTP mmW-SPRAWL project and the EC FP7-ICT IPHOBAC-NG project under grant No. 619870. L. Cavalcante thanks the Science without Borders program for its support under scholarship agreement No. 11964-13-8.